



# Reconfigurable graphene-based metamaterial polarization converter for terahertz applications

A. M. Mabrouk<sup>1</sup> · Asmaa G. Seliem<sup>2</sup> · A. A. Donkol<sup>2</sup>

Received: 17 January 2022 / Accepted: 1 September 2022 / Published online: 27 September 2022  
© The Author(s) 2022

## Abstract

This study proposes a high-gain polarization converter using a graphene-based metamaterial array, a rectangular array comprising 20 periodic unit-cell elements. Each graphene-based metamaterial unit-cell element contains a rectangular patch with four triangular-shaped graphene parts at its four corners placed over a rectangular substrate backed with a perfect electric conductor and has a relative permittivity of  $\epsilon_{sub} = 3.38$ . The metamaterial characteristics of the proposed graphene-based metamaterial unit-cell element are obtained over frequencies of 1.5–2.2 terahertz (THz). The graphene-based metamaterial array is placed over a linearly polarized slot antenna operating at 1.8 THz, with a maximum gain of 5.5 dBi. The linearly polarized wave radiated from the slot antenna can be converted into reconfigurable right-handed or left-handed circular polarizations according to the graphene parts' biasing states. Moreover, the slot antenna's operating – 10 dB bandwidth (BW) is increased by 22.2%, and the gain is enhanced to 8 dBi at the same operating frequency. A reconfigurable polarization conversion for the slot antenna can be obtained over a wide 3 dB axial ratio BW from 1.75 to 1.92 THz (20%–3 dB BW).

**Keywords** Graphene · Metamaterial · Polarization converter · Axial ratio · THz

---

This article is part of the Topical Collection on Optical and Quantum Sciences in Africa.

---

Guest edited by Salah Obayya, Alex Quandt, Andrew Forbes, Malik Maaza, Abdelmajid Belafhal and Mohamed Farhat.

---

✉ A. M. Mabrouk  
ahmed.mosaad@buc.edu.eg

Asmaa G. Seliem  
asmaa.seliem@s-mu.edu.eg

A. A. Donkol  
eng\_ahmeddonkol@yahoo.com

<sup>1</sup> Faculty of Engineering and Technology, Badr University in Cairo (BUC), Badr, Egypt

<sup>2</sup> Faculty of Engineering, Nahda University in Benisuef (NUB), Beni Suef, Egypt

## 1 Introduction

Terahertz (THz) waves are used for many applications. In medicine, THz radiation can detect differences in water content and tissue density. THz waves are used in airports for security to detect hidden illegal substances with passengers. In communication, because of their higher carrier frequency, higher data rates are achieved (up to 1000's Gbit/s data rates). In manufacturing processes, THz waves are used for imaging and sensing, quality control, and monitoring (Mukherjee and Gupta 2008). Metals, such as copper and gold, are used for antenna applications in this band (Tamagnone et al. 2012). Copper is the most used metal for antenna applications in the THz band (Keller et al. 2014), but copper-based antennas suffer high propagation losses and low radiation efficiency. These disadvantages exist as conductivity because copper's skin depth is decreased. These facts encourage using carbon-based materials, such as graphene and carbon nanotubes for THz antennas. Graphene is a two-dimensional carbon membrane with a one-atom thickness arranged in single or multiple layers (Yi and Wei 2017). Graphene material has unique characteristics. It has high electron mobility that at room temperature, approaches  $20 \text{ m}^2/\text{V}\cdot\text{s}$ . Graphene, compared with other materials, is the strongest because of its lattice configuration, and its breaking strength is 100 times that of steel. Graphene is the stiffest material ever studied, with mechanical stress of  $100 \text{ GN/m}^2$  ( $1 \times 10^{11} \text{ N/m}^2$ ) and an elastic modulus of  $1 \text{ TN/m}^2$  ( $1 \times 10^{12} \text{ N/m}^2$ ) (Sharma et al. 2021). Despite high mechanical properties, graphene has impressive flexibility (Obeng and Srinivasan 2011).

The antenna's property reconfigurability has attracted researchers' attention in wireless communications, especially mobile and satellite (Haider et al. 2013; Priya et al. 2020; Ojaroudi Parchin et al. 2020; Costantine et al. 2014). The most popular reconfigurable antenna properties are operating frequencies, the radiation pattern, and polarization (Shakhirul et al. 2019; Costantine et al. March 2015). The propagation link's budget is primarily affected because of polarization mismatch at the receiving end in most wireless communication applications, indicating that the linearly polarized (LP) wave in satellite communication might be rotated while transferring between the transmitting and receiving sides. The LP wave's rotation is the Faraday rotation, increasing the propagation link's budget (Khan and Eibert 2019). This issue decreases LP wave usage in wireless applications. Also, from the drawbacks of LP wave multipath fading during transmission and the antenna's orientation at the receiving side. Therefore, the need for circularly polarized (CP) waves became necessary because of their advantages over LP waves (Lin et al. 2020; Qi et al. 2020; Fahad et al. 2020).

The most vital advantage of CP waves is their high immunity against transmission medium effects (Baghel et al. July 2019; Tao et al. 2019; Chen and Zhang 2018). To convert an LP wave to a CP wave, researchers have designed an aided construction obeying that conversion, i.e., polarization converters. The antenna performing such conversion is a reconfigurable polarization antenna (Li et al. 2020). Reconfigurable polarization is the antenna's ability to switch between LP to left-hand circular polarization (LHCP) or right-hand circular polarization (RHCP) or between LHCP and RHCP, solving the single polarization issue in the antenna field (Liu et al. 2016; Zhang et al. 2020). Different structures can be used to convert the LP wave to the CP wave. These surfaces might be designed based on artificial magnetic conductors (AMCs) (Malhat et al. 2020) or frequency selective surfaces (Mabrouk et al. 2019). Other surfaces are based on metamaterials (MM), which are artificial structures with negative real parts of electrical permittivity ( $\epsilon$ ), magnetic permeability ( $\mu$ ), and refractive index ( $n$ ) at the antenna's operating frequency (Zheludev 2015).

The MM surface is designed as a periodic structure from the unit-cell elements satisfying metamaterial electromagnetic properties ( $\epsilon$ ,  $\mu$ , and  $n$ ). MM surfaces' operating frequency can be tuned geometrically by changing the dimensions of one or all constituent parts of the unit-cell element, changing its conductance and capacitance (Meng et al. 2020; Askari et al. 2021; Askari and Bahadoran 2022; Askari and Hosseini 2020; Tsakmakidis et al. 2007; Dani et al. 2011). The performance of the MM unit-cell elements can be changed electrically, thermally, chemically, or optically according to the material used in the proposed design (Askari et al. 2022; Smith et al. 2005). It can also be changed using positive intrinsic negative diodes, varactor diodes, or microelectromechanical systems (Yang, et al. 2021).

In this study, a graphene-based MM (GMM) unit-cell element is designed at an operating frequency of 1.8 THz. The GMM properties ( $\epsilon$ ,  $\mu$ , and  $n$ ) and the 3 dB axial ratio (AR) are calculated and figured. This unit-cell element is arranged in an MM-based surface to obtain a reconfigurable polarization dipole antenna in the THz band. A  $4 \times 4$  GMM-based array is used as a reflector for the proposed dipole antenna to convert its LP wave to LHCP or RHCP through the biasing state of each two opposite graphene triangles. The proposed constructions are designed and analyzed using a computer simulation technology (CST) microwave (MW) studio based on the finite integration technique. Section 2 presents the design and analysis of the GMM-based unit-cell element. Section 3 introduces the design and analysis of the reconfigurable polarization slot antenna. Section 4 concludes this study.

## 2 Design and analysis of GMM unit-cell element

The GMM-based unit-cell element comprises a rectangular PEC patch of a side length ( $L_p = 26.84 \mu\text{m}$ ), with four triangular-shaped graphene parts at its corners. Each graphene triangle has two equal sides of length ( $a = 10.93 \mu\text{m}$ ) and a base of length ( $b = 15.46 \mu\text{m}$ ) (Fig. 1). Two are placed oppositely at  $45^\circ$ , and the other two at  $-45^\circ$  concerning the positive  $x$ -axis. The copper patch and four graphene triangles are placed over a square-shaped substrate of side length ( $L_s = 29.82 \mu\text{m}$ ), height ( $H_s = 7.57 \mu\text{m}$ ), and relative permittivity ( $\epsilon_{r\text{sub}} = 3.38$ ), backed by a square perfect electric conductor (PEC) ground plane of the same side length.

Graphene's controllable conductivity ( $\sigma(\omega)$ ) is a critical property for antenna reconfigurability applications. Unlike most popular materials, graphene conductivity can be altered

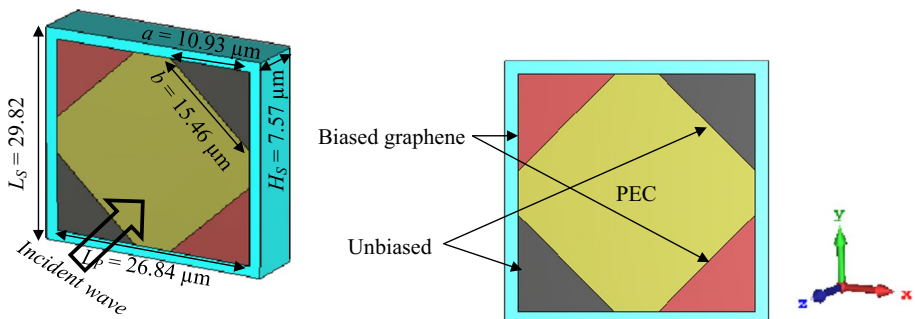


**Fig. 1** A 3D diagram of the graphene-based metamaterial (GMM) unit-cell element

in diverse ways, such as applied electric field, applied direct current (DC) voltage, or chemical doping. The Kubo formula represents the graphene conductivity as a frequency-dependent complex value according to Eq. (1) (Hu and Wang 2018).

$$\sigma(\omega) = \sigma_{inter}(\omega) + \sigma_{intra}(\omega) \tag{1}$$

where  $\sigma_{inter}(\omega)$  is the inter-band contribution corresponding to electron–hole pair generation and recombination events.  $\sigma_{intra}(\omega)$  is the intra-band contribution corresponding to the conductivity of free carriers. Each inter-band and intra-band is represented as:

$$\sigma_{inter}(\omega, \mu_c, \Gamma, T) \approx j \frac{q_e^2}{4\pi\hbar} \ln\left(\frac{2|\mu_c| - (\omega + j\tau^{-1})\hbar}{2|\mu_c| + (\omega + j\tau^{-1})\hbar}\right) \tag{2}$$

and

$$\sigma_{intra}(\omega, \mu_c, \Gamma, T) \approx -j \frac{q_e^2 K_B T}{\pi\hbar^2(\omega - j2\Gamma)} \times \left(\frac{\mu_c}{K_B T} + \ln(e^{-\mu_c/K_B T} + 1)\right)^2 \tag{3}$$

where  $\omega$  is the angular frequency,  $\mu_c$  is the chemical potential (between 0 and 2 eV),  $\Gamma$  is the scattering rate ( $\Gamma = 1/\tau$ ),  $T$  is the temperature (K),  $\tau$  is the time of relaxation,  $q_e$  is the electron charge,  $K_B$  is the Boltzmann’s constant, and  $\hbar$  is the reduced Plank’s constant.

For operating frequencies below 8 THz, graphene conductivity can be represented in terms of the inter-band only where the intra-band can be neglected (Hu and Wang 2018). The most well-known technique used to control graphene conductivity is by varying the applied DC voltage (Hu and Wang 2018). In this study, we apply the graphene conductivity inter-band because it is designed for applications below 8 THz. According to Eq. (2), the graphene functions as a dielectric if it is unbiased with the DC voltage value equivalent to  $\mu_c = 0$  (unbiased state). However, it functions as a conductor if it is biased with the DC voltage value equivalent to  $\mu_c = 2eV$  (unbiased state). In this study, we discuss the biased and unbiased states of graphene to achieve the polarization conversion property, as discussed below.

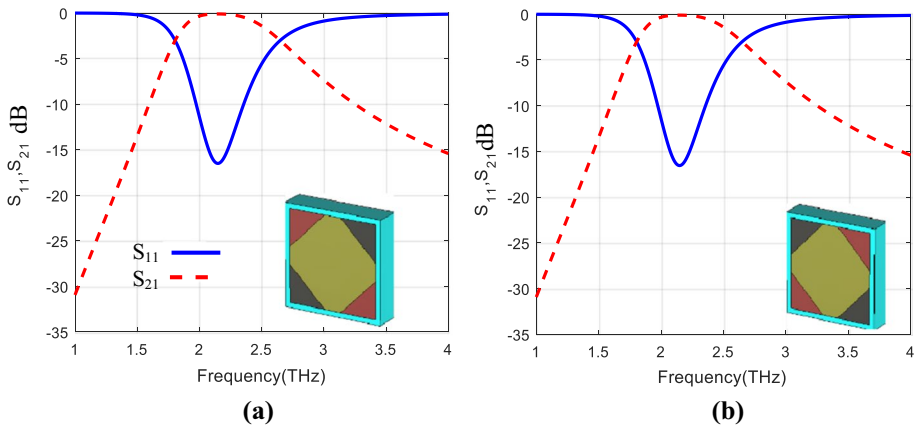


**Fig. 2** The reflection and transmission coefficient variations versus the GMM unit-cell element frequency when **a** the two opposite graphene triangles directed to  $\theta_1 = +45^\circ$  are biased and **b** directed to  $\theta_2 = -45^\circ$  are biased

Also, the resistivity of graphene monolayer has a large dependency on the temperature. According to several measurements, it was found that for temperatures lower than 150 K, the graphene monolayer resistivity is linearly dependent on temperature. For higher temperatures degrees the dependency of graphene resistivity on temperature is strongly increased. This may be as a result of ripples in the graphene monolayer or coupling between it and the remote interfacial phonons (RIPs) at the SiO<sub>2</sub> surface (Price et al. 2012).

Using a Floquet port in the CST-MW software, the unit-cell element's dimensions are optimized and analyzed. The two opposite graphene triangles directed to  $\theta_1 = +45^\circ$  are biased, and those directed to  $\theta_1 = -45^\circ$  are unbiased (case 1). Figure 2a shows the magnitudes of reflection ( $S_{11}$ ) and transmission ( $S_{21}$ ) coefficients of the GMM unit-cell element. Conversely, in case 2, the two opposite graphene triangles directed to  $\theta_2 = -45^\circ$  are biased, and those directed to  $\theta_2 = +45^\circ$  are unbiased. Figure 2b shows the magnitudes of reflection ( $S_{11}$ ) and transmission ( $S_{21}$ ) coefficients of the GMM unit-cell element. Note that  $S_{11}$  and  $S_{21}$  have the same value at 1.8 THz. Figure 3 shows the variation of the reflection ( $P_{11}$ ) and the transmission ( $P_{21}$ ) phases and their differences in the two cases. From the results, the phase difference in both cases is ( $\varphi = 90^\circ$ ) at the operating frequency, and the proposed

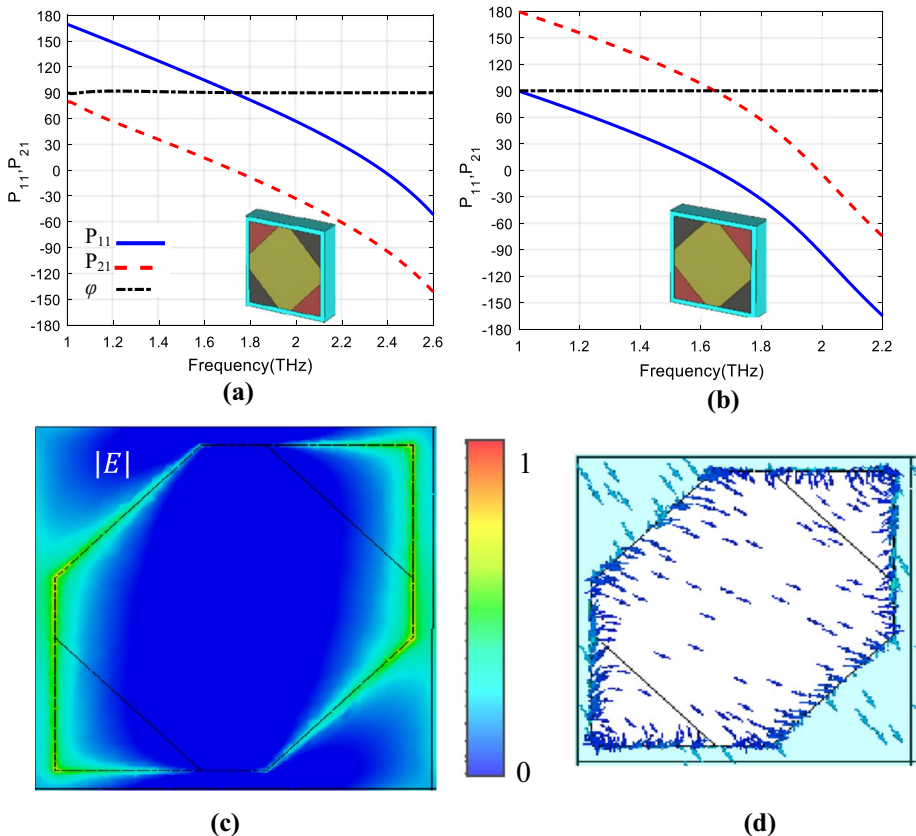


**Fig. 3** The reflection and transmission phase variations and their difference versus the MM unit-cell element frequency when **a** the two opposite graphene triangles directed to  $\theta_1 = +45^\circ$  are biased, **b** directed to  $\theta_2 = -45^\circ$  are unbiased, **c** Electric field map, and **d** the charge distribution for the GMM unit-cell element case 2

GMM unit-cell element satisfies the AMC requirements at the operating frequency of 1.8 THz (Sofi et al. 2019). Figures 3c, and d presents the electric field map and the distribution of the charge distribution, respectively, for the proposed GMM unit-cell element case (2) resonance excitation and concentration through the patch area of the unit-cell at the frequency of 1.8 THz. The charges are mainly concentrated at the tips of the biased graphene triangles only (case 2) like in Ahmadivand et al. (2016).

The reflection  $S_{11}$  and transmission  $S_{21}$  coefficients are used to calculate the MM parameters ( $\epsilon$ ,  $\mu$ , and  $n$ ) for the unit-cell element. First, the impedance  $z$  and the refractive index  $n$  are calculated using Eqs. (4) and (5), respectively (Zheludev 2015).

$$z = \pm \sqrt{\frac{(1 + T_{xx})^2 - T_{xy}^2}{(1 - T_{xx})^2 - T_{xy}^2}} \tag{4}$$

$$n = \frac{1}{kH} \cos^{-1} \left[ \frac{1}{2T_{xy}} (1 - T_{xx}^2 + T_{xy}^2) \right] \tag{5}$$

$n$  is the refractive index,  $k$  is the incident wave’s wavenumber, and  $H$  is the MM unit-cell element’s overall thickness. These two equations are used to calculate the electrical permittivity,  $\epsilon$ , and the magnetic permeability  $\mu$  as in Eqs. (6) and (7), respectively [31, 232].

$$\epsilon = n/z \tag{6}$$

$$\mu = n \times z \tag{7}$$

Figures 4, 5, and 6 show the variations of real and imaginary parts of the unit-cell element’s parameters ( $\epsilon$ ,  $\mu$ , and  $n$ ) versus frequency, respectively. The real parts of  $\epsilon$ ,  $\mu$ , and  $n$  of the MM unit-cell elements must be negative at the operating frequency of 1.8 THz in this study. In Fig. 4a, the real part of the relative permittivity  $\epsilon$  has negative values through a wide band of frequencies from 1.5 to 2.2 THz for case 1 and 1.6 to 2.1 THz for case 2.

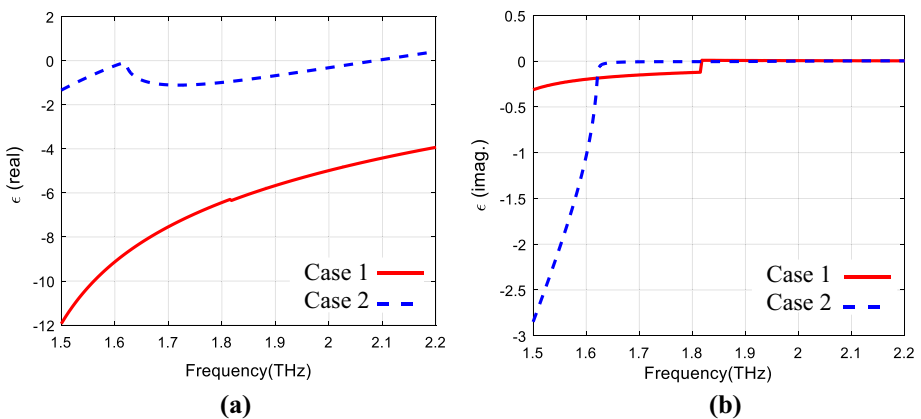


**Fig. 4** The variations of **a** the real part and **b** the imaginary part of permittivity versus the GMM unit-cell element’s frequency for cases 1 and 2, respectively

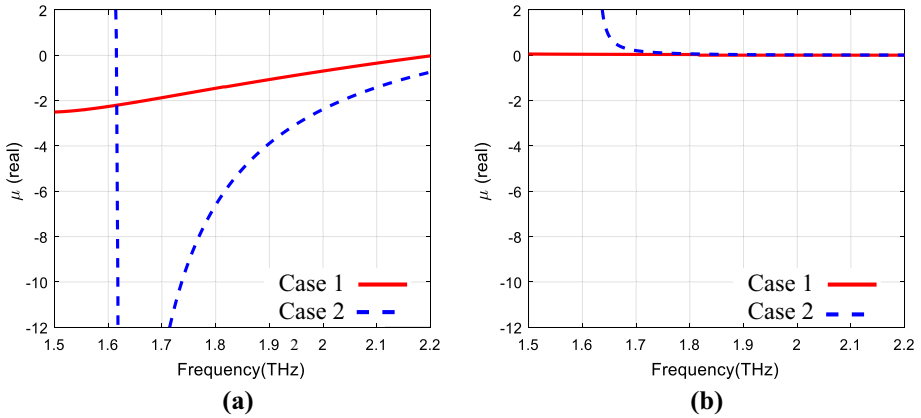


**Fig. 5** The variations of **a** the real part and **b** the imaginary part of permittivity versus the GMM unit-cell element's frequency for cases 1 and 2, respectively

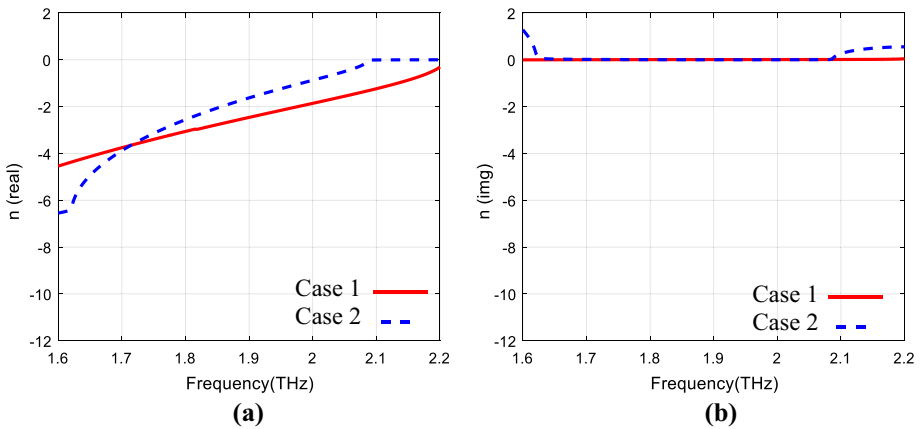


**Fig. 6** The variations of **a** the real part and **b** the imaginary part of the refractive index versus the GMM unit-cell element's frequency for cases 1 and 2, respectively

Figure 5a shows that the real part of the relative magnetic permeability  $\mu$  has negative values over the frequency band from 1.5 to 2.2 THz for case 1 and 1.6 to 2.2 THz for case 2.

Also, the proposed GMM unit-cell element has negative values for the refractive index  $n$  through the frequency band from 1.6 to 2.2 THz for cases 1 and 2 (Fig. 6a). Here, the proposed unit-cell element is valid to be an MM unit cell.

From the results, the proposed GMM unit-cell element can be used for polarization conversion at 1.8 THz. For case 1, because the reflection phase  $P_{11}$  is greater than the

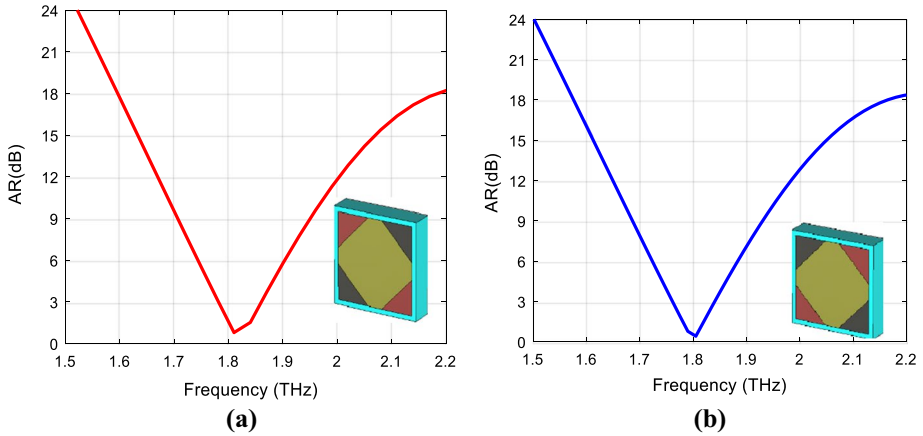


**Fig. 7** The variations of the axial ratio (AR) versus frequency for **a** the RHCP GMM unit-cell element (case 1) and **b** the LHCP GMM unit-cell element (case 2)

transmission phase  $P_{21}$  by  $90^\circ$  (Fig. 3a), the transmitted wave’s polarization is RHCP. For case 2, because the transmitted phase  $P_{21}$  is greater than the reflection phase  $P_{11}$  by  $90^\circ$  (Fig. 3b), the transmitted wave’s polarization is LHCP (Dani et al. 2011).

In summary, the proposed GMM unit-cell element converted the incident LP to RHCP or LHCP according to the biasing state of the graphene triangles as in cases 1 and 2. The 3 dB AR bandwidth (BW) from 1.78 to 1.86 THz (4.4% 3 dB BW) is achieved for case 1 (Fig. 7a). The 3 dB AR BW from 1.76 to 1.84 THz (4.44% 3 dB BW) is achieved for case 2 (Fig. 7b). The AR is calculated using Eq. (8) (Price et al. 2012).

$$AR = \sqrt{\frac{1 + \beta^2 + \sqrt{(1 - \beta^2)^2 + 4\beta^2 \cos^2 \varphi}}{1 + \beta^2 - \sqrt{(1 - \beta^2)^2 + 4\beta^2 \cos^2 \varphi}}} \tag{8}$$

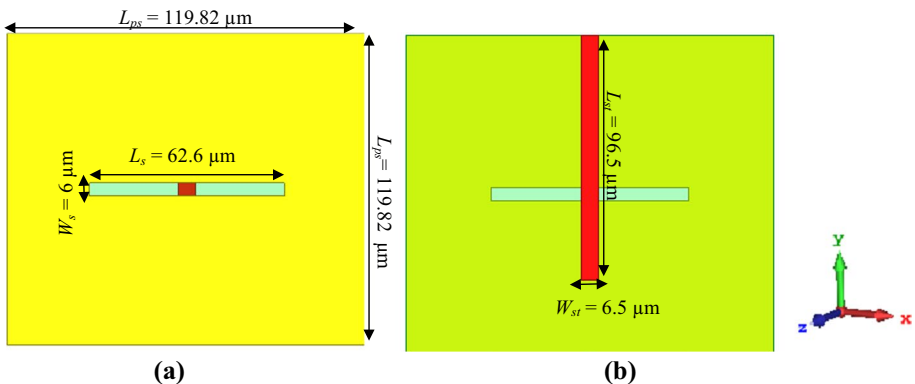


**Fig. 8** **a** The top view and **b** the bottom view of the LP slot antenna



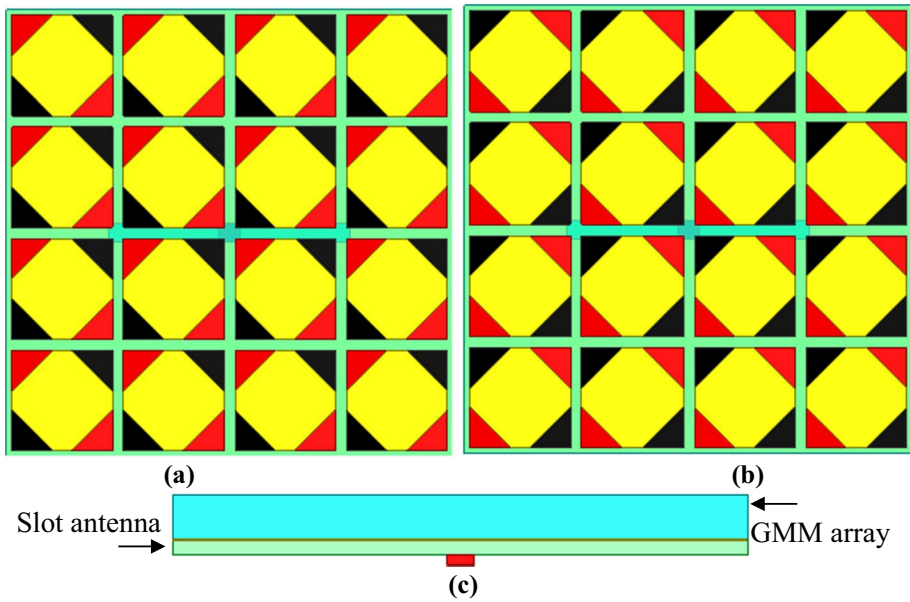


**Fig. 9** 4×4 GMM unit-cell elements array over the proposed slot antenna for graphene biasing states for cases **a** 1 and **b** 2, and **c** is the side view of the overall construction

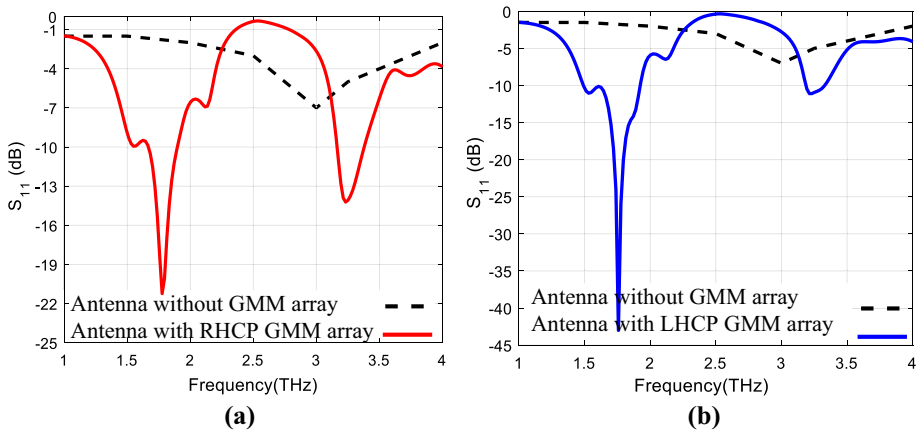


**Fig. 10** Variations of the reflection coefficient versus the slot antenna's frequency against that of the overall construction with biased GMM array for **a** cases 1 and **b** 2

where  $\beta = \frac{|T_{xx}|}{|T_{xy}|}$  and  $\varphi$  is the phase difference between  $T_{xx}$  and  $T_{xy}$ .

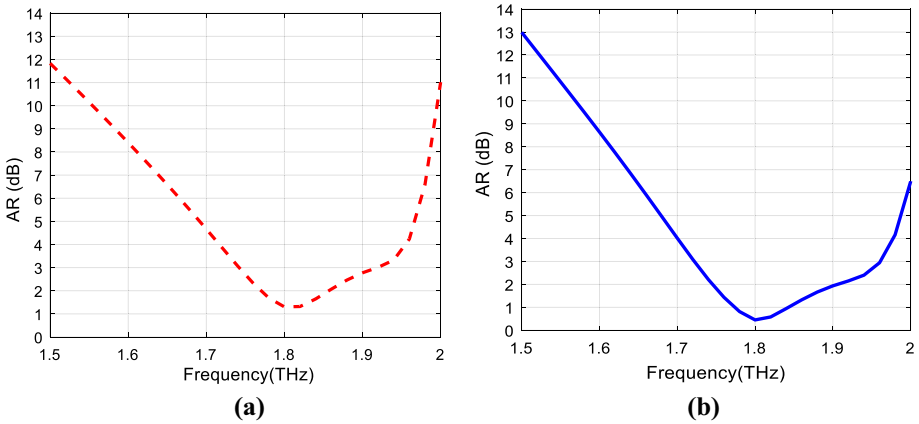


Fig. 11 The AR of the overall construction with biased GMM array for **a** cases 1 and **b** 2

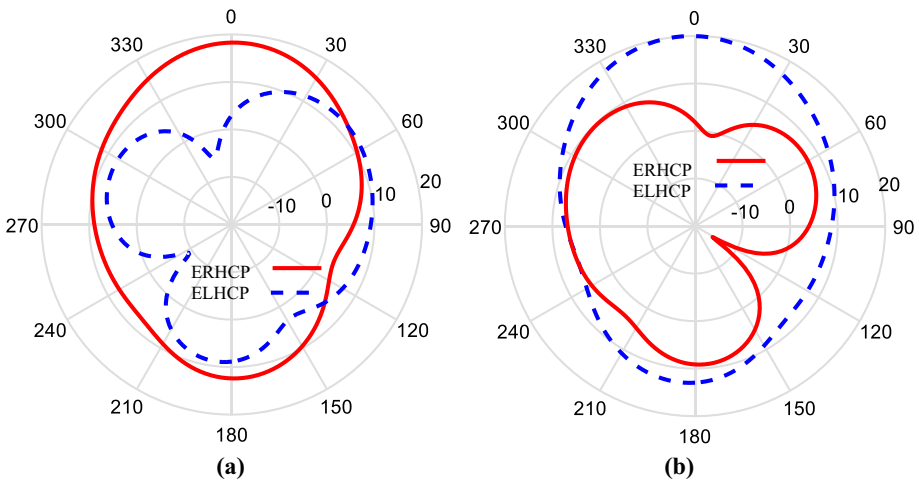


Fig. 12 The  $E_R$  and the  $E_L$  of the overall construction with biased GMM array for **a** cases 1 and **b** 2

### 3 Reconfigurable polarization slot antenna using a GMM array

The proposed GMM unit-cell element is arranged in a  $4 \times 4$  array to perform polarization conversion for an LP slot antenna comprising a square PEC sheet of a side length  $L_{ps} = 119.82 \mu\text{m}$  and a rectangular slot of length  $L_s = 62.6 \mu\text{m}$  and width of  $W_s = 6 \mu\text{m}$ . The PEC sheet with the rectangular slot is placed over a square substrate of the same side length (height of  $H_s = 2.5 \mu\text{m}$ ) and relative permittivity  $\epsilon_{rs} = 3.38$  (Fig. 8a). The slot antenna is radiated through a stripline placed at the bottom of the substrate with length  $L_{st} = 96.5 \mu\text{m}$  and width  $W_{st} = 6.5 \mu\text{m}$  (Fig. 8b).

An array of  $4 \times 4$  GMM unit-cell elements with a surface area of  $119.82 \times 119.82 \mu\text{m}^2$  is used as a polarization converter for the proposed slot antenna (Fig. 9a). This array is placed under the proposed dipole antenna at an optimized distance  $h = 25 \mu\text{m}$ , equivalent to  $\lambda/4$ . The reflected wave from the MM array is of a high gain with a maximum value of 6.18 dBi

along the positive  $z$ -axis (Fig. 10b), with a wide BW from 1.5 to 2.1 THz (30.93%,  $-10$  dB BW) (Fig. 11a). Note that the  $-10$  dB BW and the gain of the proposed dipole antenna are enhanced considerably.

Figure 10a shows that the reflection coefficient of the overall construction is enhanced to  $-22$  dB instead of  $-2$  dB of the slot antenna when the graphene triangles are biased in case 1 and enhanced to  $-44$  dB when the graphene triangles are biased in case 2 (Fig. 10b). The enhancement of the reflection coefficient of the proposed slot antenna at the operating frequency (1.8 THz) means increasing the matching level between the antenna and the GMM array. As a result of the enhanced matching level, the antenna gain is also increased in both cases 1 and 2 as shown in Fig. 11.

Moreover, the transmitted wave from the GMM array is converted to RHCP and LHCP waves for cases 1 (Fig. 11) and 2 (Fig. 12), respectively.

The slot antenna's LP wave is converted to RHCP when the GMM array's graphene is biased according to case 1. This is confirmed by the results of Fig. 11a, where a wide 3 dB BW of 10.55% and from 1.74 to 1.93 THz is achieved. Also, the ERHCP component of the radiated field is greater than the ELHCP component by 18 dB at the operating frequency of 1.18 THz (Fig. 12a). Biasing the GMM array's graphene according to case 2 produces an LHCP wave with a 3 dB AR BW of 13.3% from 1.73 to 1.96 THz (Fig. 11b). The difference between the ERHCP and LHCP components of the radiated field for this case is 19 dB at the operating frequency of 1.8 THz (Fig. 12b).

Compared with similar studies (Tsakmakidis et al. 2007; Dani et al. 2011), the proposed configuration exhibits an electrical polarization conversion with a wider BW, better CP conversion, more simplicity, and a wide 3 dB AR bandwidth.

## 4 Conclusions

A GMM unit-cell element was designed and analyzed at 1.8 THz. A high gain with a reconfigurable polarization antenna was introduced using a GMM array. The GMM array comprised 20 GMM unit-cell elements arranged over the proposed slot antenna. Using the GMM array increased the  $-10$  dB BW by 22.2%, and the gain of the proposed slot antenna was enhanced to 8 dBi instead of 5.8 dBi. Moreover, the GMM polarization converter switched the slot antenna's LP wave between RHCP and LHCP waves according to the graphene materials' biasing states of cases 1 and 2 with a high 3 dB AR BW (10.55% and 13.3%, respectively).

**Funding** Open access funding provided by The Science, Technology & Innovation Funding Authority (STDF) in cooperation with The Egyptian Knowledge Bank (EKB). The authors have not disclosed any funding.

## Declarations

**Conflict of interest** The authors declare that they have no known competing financial interests or personal relationships that could have appeared to influence the work reported in this paper.

**Open Access** This article is licensed under a Creative Commons Attribution 4.0 International License, which permits use, sharing, adaptation, distribution and reproduction in any medium or format, as long as you give appropriate credit to the original author(s) and the source, provide a link to the Creative Commons licence, and indicate if changes were made. The images or other third party material in this article

are included in the article's Creative Commons licence, unless indicated otherwise in a credit line to the material. If material is not included in the article's Creative Commons licence and your intended use is not permitted by statutory regulation or exceeds the permitted use, you will need to obtain permission directly from the copyright holder. To view a copy of this licence, visit <http://creativecommons.org/licenses/by/4.0/>.

## References

- Ahmadivand, A., Sinha, R., Gerislioglu, B., Karabiyik, M., Pala, N., Shur, M.: Transition from capacitive coupling to direct charge transfer in asymmetric terahertz plasmonic assemblies. *Opt. Lett.* **41**, 5333–5336 (2016)
- Askari, M., Bahadoran, M.: A refractive-index-based microwave sensor based on classical electromagnetically induced transparency in metamaterials. *Optik* **253**, 168589 (2022)
- Askari, M., Hosseini, M.V.: A novel metamaterial design for achieving a large group index via classical electromagnetically induced reflectance. *Opt. Quant. Electron.* **52**(4), 1–17 (2020)
- Askari, M., Pakarzadeh, H., Shokrgozar, F.: High Q-factor terahertz metamaterial for superior refractive index sensing. *JOSA B* **38**(12), 3929–3936 (2021)
- Askari, M., Touhidi Nia, Z., Hosseini, M.V.: Modified fishnet structure with a wide negative refractive index band and a high figure of merit at microwave frequencies. *J. Opt. Soc. Am.* **39**, 1282–1288 (2022)
- Baghel, A.K., Kulkarni, S.S., Nayak, S.K.: Linear-to-cross-polarization transmission converter using ultrathin and smaller periodicity metasurface. *IEEE Antennas Wirel. Propag. Lett.* **18**(7), 1433–1437 (2019). <https://doi.org/10.1109/LAWP.2019.2919423>
- Chen, Q., Zhang, H.: Dual-patch polarization conversion metasurface-based wideband circular polarization slot antenna. *IEEE Access* **6**, 74772–74777 (2018). <https://doi.org/10.1109/ACCESS.2018.2883992>
- Costantine, J., Tawk, Y., Christodoulou, C.G.: Reconfigurable antennas: Reconfigurable Antennas and Their Applications. In: Chen, Z.N. (ed.) *Handbook of Antenna Technologies*, pp. 1–30. Springer Singapore, Singapore (2014)
- Costantine, J., Tawk, Y., Barbin, S.E., Christodoulou, C.G.: Reconfigurable antennas: design and applications. *Proc. IEEE* **103**(3), 424–437 (2015). <https://doi.org/10.1109/JPROC.2015.2396000>
- Dani, K.M., Zahyun, K., Upadhyay, P.C., Prasankumar, R.P., Taylor, A.J., Brueck, S.R.J.: Ultrafast non-linear optical spectroscopy of a dual-band negative index metamaterial all-optical switching device. *Opt. Express* **19**(5), 3973–3983 (2011)
- Fahad, A.K., et al.: Ultra-thin metasheet for dual-wide-band linear to circular polarization conversion with wide-angle performance. *IEEE Access* **8**, 163244–163254 (2020). <https://doi.org/10.1109/ACCESS.2020.3021425>
- Haider, N., Caratelli, D., Yarovoy, A.G.: Recent developments in reconfigurable and multiband antenna technology. *Int. J. Antennas Propag.* **2013**, 869170 (2013)
- Hu, X., Wang, J.: Design of graphene-based polarization-insensitive optical modulator. *Nanophotonics* **7**(3), 651–658 (2018). <https://doi.org/10.1515/nanoph-2017-0088>
- Keller, S.D., Zaghoul, A.I., Shanov, V., Schulz, M.J., Mast, D.B., Alvarez, N.T.: Electromagnetic simulation and measurement of carbon nanotube thread dipole antennas. *IEEE Trans. Nanotechnol.* **13**(2), 394–403 (2014). <https://doi.org/10.1109/TNANO.2014.2306330>
- Khan, S., Eibert, T.F.: A dual-band metasheet for asymmetric microwave transmission with polarization conversion. *IEEE Access* **7**, 98045–98052 (2019). <https://doi.org/10.1109/ACCESS.2019.2929115>
- Li, Y., Zhang, H., Yang, T., Sun, T., Zeng, L.: A multifunctional polarization converter base on the solid-state plasma metasurface. *IEEE J. Quantum Electron.* **56**(2), 1–7 (2020). <https://doi.org/10.1109/JQE.2020.2975019>
- Lin, B., Lv, L., Guo, J., Liu, Z., Ji, X., Wu, J.: An ultra-wideband reflective linear-to-circular polarization converter based on anisotropic metasurface. *IEEE Access* **8**, 82732–82740 (2020). <https://doi.org/10.1109/ACCESS.2020.2988058>
- Liu, Y., Hao, Y., Li, K., Gong, S.: Radar cross section reduction of a microstrip antenna based on polarization conversion metamaterial. *IEEE Antennas Wirel. Propag. Lett.* **15**, 80–83 (2016). <https://doi.org/10.1109/LAWP.2015.2430363>
- Mabrouk, A.M., Malhat, H.A., Zainud-Deen, S.H.: *Electronic Beam Switching Using Graphene-Based Frequency Selective Surface*. In: 2019 36th National Radio Science Conference (NRSC), pp. 68–75: IEEE (2019)

- Malhat, H.-A., Mabrouk, A.M., El-Hmaily, H., Hamed, H.F., Zainud-Deen, S.H., Ibrahim, A.A.E.M.: Electronic beam switching using graphene artificial magnetic conductor surfaces. *Opt. Quantum Electron.* **52**(7), 357 (2020)
- Meng, Y., Wang, J., Chen, H., Zheng, L., Ma, H., Qu, S.: Countering single-polarization radar based on polarization conversion metamaterial. *IEEE Access* **8**, 206783–206789 (2020). <https://doi.org/10.1109/ACCESS.2020.3034927>
- Mukherjee, P., Gupta, B.: Terahertz (THz) frequency sources and antennas—A brief review. *Int. J. Infrared Millimeter Waves* **29**(12), 1091–1102 (2008)
- Obeng, Y., Srinivasan, P.: Graphene: is it the future for semiconductors? An overview of the material, devices, and applications. *Interface Mag.* **20**(1), 47–52 (2011)
- Parchin, N.O., Basherlou, H.J., Al-Yasir, Y.I.A., Abdulkhaleq, A.M., Abd-Alhameed, R.A.: Reconfigurable antennas: switching techniques—a survey. *Electronics* **9**(2), 336 (2020)
- Price, A.S., Hornett, S.M., Shytov, A.V., Hendry, E., Horsell, D.W.: Nonlinear resistivity and heat dissipation in monolayer graphene. *Phys. Rev. B* **85**(16), 161411 (2012)
- Priya, A., Kaja Mohideen, S., Saravanan, M.: Multi-state reconfigurable antenna for wireless communications. *J. Electr. Eng. Technol.* **15**(1), 251–258 (2020)
- Qi, Y., Zhang, B., Liu, C., Deng, X.: Ultra-broadband polarization conversion meta-surface and its application in polarization converter and RCS reduction. *IEEE Access* **8**, 116675–116684 (2020). <https://doi.org/10.1109/ACCESS.2020.3004127>
- Shakhirul, M.S., Jusoh, M., Lee, Y.S., Nurol Husna, C.R.: A review of reconfigurable frequency switching technique on microstrip antenna. *J. Phys. Conf. Ser.* **1019**, 012042 (2018)
- Sharma, N., Gupta, R.D., Sharma, R.C., Dayal, S., Yadav, A.S.: Graphene: An overview of its characteristics and applications. *Mater. Today Proc.* **47**, 2752–2755 (2021). <https://doi.org/10.1016/j.matpr.2021.03.086>
- Smith, D.R., Vier, D.C., Koschny, Th., Soukoulis, C.M.: Electromagnetic parameter retrieval from inhomogeneous metamaterials. *Phys. Rev. E* **71**(3), 036617–036628 (2005)
- Sofi, M.A., Saurav, K., Koul, S.K.: Reconfigurable polarization converter printed on single substrate layer frequency selective surface. In: 2019 IEEE MTT-S International Microwave and RF Conference (IMARC), pp. 1–4: IEEE (2019)
- Tamagnone, M., Gómez-Díaz, J.S., Perruisseau-Carrier, J., Mosig, J.R.: Analysis and design of terahertz antennas based on plasmonic resonant graphene sheets. *J. Appl. Phys.* **112**(11), 114915–1149154 (2012)
- Tao, Z., Zhang, H., Xu, H., Chen, Q.: Novel Polarization Conversion Metasurface Based Circular Polarized Slot Antenna with Low Profile. In: 2019 Cross Strait Quad-Regional Radio Science and Wireless Technology Conference (CSQRWC), Taiyuan, China, pp. 1-3. <https://doi.org/10.1109/CSQRWC.2019.8799106> (2019)
- Tsakmakidis, K.L., Boardman, A.D., Hess, O.: ‘Trapped rainbow’ storage of light in metamaterials. *Nature* **450**(7168), 397–401 (2007)
- Yang, Z., et al.: Reconfigurable multifunction polarization converter integrated with PIN Diode. *IEEE Microw. Wireless Compon. Lett.* **31**(6), 557–560 (2021). <https://doi.org/10.1109/LMWC.2021.3064039>
- Yi, D., Wei, X.: Recent developments of tunable microwave absorbers using graphene. In: 2017 Sixth Asia-Pacific Conference on Antennas and Propagation (APCAP), pp. 1–3. <https://doi.org/10.1109/APCAP.2017.8420527> (2017)
- Zhang, X., Chen, C., Jiang, S., Wang, Y., Chen, W.: A high-gain polarization reconfigurable antenna using polarization conversion metasurface. *Prog. Electromagn. Res. C* **105**, 1–10 (2020). <https://doi.org/10.2528/PIERC20052001>
- Zheludev, N.I.: Obtaining optical properties on demand. *Science* **348**(6238), 973–974 (2015)